Bulletin of the Seismological Society of America, Vol. 92, No. 8, pp. 3309–3317, December 2002

Predominance of Unilateral Rupture for a Global Catalog of Large Earthquakes

by Jeffrey J. McGuire,* Li Zhao, and Thomas H. Jordan

Abstract The manner in which an earthquake rupture propagates across a fault reflects both the initial properties of the fault and the dynamical stresses produced by the rupture. We quantify the propagation of an earthquake rupture using the second moments of the earthquake space–time distribution. In particular, the second moments provide a simple way to differentiate between approximately bilateral and predominantly unilateral ruptures. We determined the second moments for a catalog of $M_w \geq 7$ earthquakes that have occurred since 1994. The results show that approximately 80% of large shallow ruptures are predominantly unilateral. Our result agrees well with strong-motion inversions from previous studies on moderate and large earthquakes. The predominance of unilateral propagation in large earthquakes is explained by a simple characteristic earthquake model in which large events rupture an entire structurally defined fault segment and nucleation points are uniformly distributed along the fault. The predominance of unilateral rupture may also be enhanced by the dynamic stress field produced by contrasts in the elastic properties between the two sides of plate boundary faults.

Introduction

There is great variety in the manner in which an earthquake rupture spreads across a fault. The 1992 M_w 7.2 Landers earthquake nucleated at the southern end of the Johnson Valley fault and propagated almost exclusively to the northwest (Wald and Heaton, 1994). In contrast, the 1989 M_w 6.8 Loma Prieta earthquake nucleated in the center of its rupture area and then propagated to both the northwest and southeast along strike (Beroza, 1995; Wald *et al.*, 1991). Although the fundamental difference between these two styles of rupture, unilateral (Landers) versus bilateral (Loma Prieta), is clear from estimates of their slip distributions, it is not often quantified. Earthquake catalogs represent earthquakes as point sources (either epicenter or centroid) and hence contain no information about their rupture propagation.

To quantify where a particular earthquake lies on the scale ranging from bilateral to unilateral, we use the simplest representation of an earthquake that contains information about rupture directivity, the point-source representation plus the second-degree moments (Backus and Mulcahy, 1976a,b; Backus, 1977a). Assuming a constant moment tensor during rupture ($\mathbf{M}(\mathbf{r}, t) = \hat{\mathbf{M}} f(\mathbf{r}, t)$), the second-degree moments, which include the spatial and temporal variances of the moment-release distribution, are defined as

$$\hat{\boldsymbol{\mu}}^{(2,0)} = \iint \dot{f}(\mathbf{r},t)(\mathbf{r} - \mathbf{r}_0)(\mathbf{r} - \mathbf{r}_0)^T dV dt, \qquad \hat{\mu}^{(0,2)} = \iint \dot{f}\,(\mathbf{r},t)(t - t_0)^2\, dV dt, \tag{1}$$

$$\hat{\boldsymbol{\mu}}^{(1,1)} = \iint \dot{f}(\mathbf{r},t)(\mathbf{r} - \mathbf{r}_0)(t - t_0) dV dt, \tag{2}$$

where $\dot{f}(\mathbf{r}, t)$ is the scalar source–space–time function that describes the spatial and temporal distribution of moment release, and $(\mathbf{r}_0, t_0)$ denote the spatial and temporal centroids. $\hat{\boldsymbol{\mu}}^{(2,0)}$ and $\hat{\mu}^{(0,2)}$ denote the second central spatial and temporal moments, and the mixed moment, $\hat{\boldsymbol{\mu}}^{(1,1)}$, which is analogous to the directivity parameter of Ben-Menahem (1961), describes the overall rupture directivity (McGuire *et al.*, 2001).

For a general source model where the moment tensor varies in space and time, the second moments are a fourth-order tensor that cannot be uniquely determined from the displacement field Backus (1977a,b). In this case, the quantities $\hat{\boldsymbol{\mu}}^{(2,0)}$, $\hat{\mu}^{(0,2)}$, and $\hat{\boldsymbol{\mu}}^{(1,1)}$ represent the projection of the full fourth-order tensor through the average moment tensor, $\hat{\mathbf{M}}$. A similar projection is necessary to define a centroid location for a general source model (see Dahlen and Tromp, [1988], p. 169). Bukchin (1995) showed that in the case of a constant moment tensor, the second-order moments of $\dot{f}(\mathbf{r}, t)$ are uniquely determined from the displacement field.

*Present address: Department of Geology and Geophysics, Woods Hole Oceanographic Institution, Woods Hole, Massachusetts 02543.

Although in detail many, if not all, earthquakes have deviations from a constant moment tensor, the effect on the low-frequency wave field is usually small at least compared to the noise caused by lateral heterogeneity. Riedesel and Jordan (1989) searched a catalog of 60 earthquakes for frequency dependence of the seismic moment tensor at low frequencies ($\leq$11 mHz) but found none that were statistically significant. Thus, although the quantities we determine are a projection through this average moment tensor, they are still interpretable in terms of the location and dimensions of the source volume.

The values of $\hat{\boldsymbol{\mu}}^{(2,0)}$ and $\hat{\boldsymbol{\mu}}^{(1,1)}$ for the Landers earthquake slip distribution determined by Wald and Heaton (1994) are shown in Figure 1 along with the surface trace of the Landers rupture. The overall northwestward directivity of this event leads to the $\hat{\boldsymbol{\mu}}^{(1,1)}$ vector pointing along the strike of the fault to the northwest. The second spatial moment can be represented as a three-dimensional ellipsoid that contains the characteristic rupture volume. The surface projection of this ellipse for the Landers event denotes the portion of the fault that produced the majority of the seismic moment release in this event (Fig. 1).

Following Backus (1977a) and Silver and Jordan (1983), we define the characteristic dimension, $x_c(\hat{\mathbf{n}})$, of the slip distribution in a direction $\hat{\mathbf{n}}$, the characteristic duration τ_c, the characteristic length L_c, the characteristic (or apparent rupture) velocity v_c, and the average velocity of the instantaneous spatial centroid, v_0:

$$x_c(\hat{\mathbf{n}}) = 2\sqrt{\hat{\mathbf{n}}^T\left[\hat{\boldsymbol{\mu}}^{(2,0)}/M_0\right]\hat{\mathbf{n}}}, \quad \tau_c = 2\sqrt{\hat{\mu}^{(0,2)}/M_0}, \qquad v_c = L_c/\tau_c, \quad \mathbf{v}_0 = \hat{\boldsymbol{\mu}}^{(1,1)}/\hat{\mu}^{(0,2)}, \tag{3}$$

where M_0 is the seismic moment and $x_c(\hat{\mathbf{n}})$ has its maximum value, L_c, when $\hat{\mathbf{n}}$ corresponds to the eigenvector associated with the largest eigenvalue of $\hat{\boldsymbol{\mu}}^{(2,0)}$. Another way to express the magnitude of the directivity in a rupture is through the characteristic propagation distance of the centroid, $L_0 = v_0\tau_c$. Owing to the weighted average nature of the second moments, the characteristic dimensions of a rupture are always smaller than its total dimensions, but they provide an estimate of the region that contributed significantly to the moment release.

For a unilateral (Haskell) rupture where slip nucleates at one end of a rectangular fault and propagates to the other at a rupture velocity v with a uniform slip distribution, $v_c = v_0 = v$. However, for a symmetric bilateral rupture that initiates in the middle and propagates to both ends of a fault at rupture velocity v with a uniform slip distribution, $v_c = 2v$ and $v_0 = 0$ because the instantaneous centroid does not move during the rupture. Thus, although these two cases have the same static (final) slip distribution, their kinematical differences are apparent in the relative magnitudes of v_c and v_0, or equivalently, L_c and L_0.

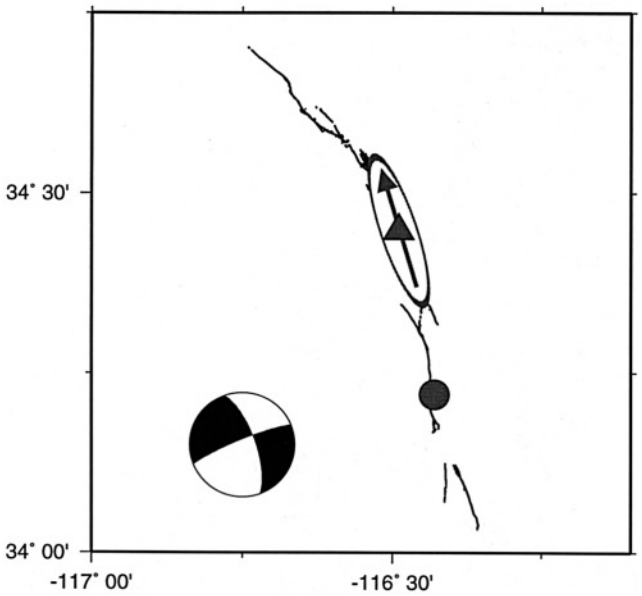

Figure 1. Map of the 1992 Landers earthquake region. The triangle and circle denote the event's centroid location and epicenters, respectively. The gray ellipses represents the second spatial moment, $\hat{\boldsymbol{\mu}}^{(2,0)}$, and the arrow represents the mixed moment between space and time, $\hat{\boldsymbol{\mu}}^{(1,1)}$ (scaled to the length of $v_0\tau_c$), which were computed from the slip model of Wald and Heaton (1994). $\hat{\boldsymbol{\mu}}^{(1,1)}$ describes the overall directivity of the event, which was to the northwest along the strike of the fault.

The slip distributions determined for the Loma Prieta and the Landers earthquakes differ significantly in their relative magnitudes of v_c and v_0. The Landers event slip distribution determined by Wald and Heaton (1994) has a v_c of 2.8 km/sec and a v_0 of 2.2 km/sec. Thus the directivity ratio v_0/v_c, which ranges from 0 for a symmetric bilateral rupture to 1 for a uniform-slip unilateral rupture, is about 0.79 for Landers, confirming its well-known unilateral nature. For Loma Prieta, the ratio of v_0/v_c was much smaller, confirming its qualitatively bilateral rupture. Owing to differences between the slip models in the strengths of the two main asperites, the directivity ratio for Loma Prieta ranges from 0.1 (Wald *et al.*, 1991) to 0.47 (Beroza, 1995). Thus, bilateral ruptures correspond to $v_0/v_c \leq\sim 0.5$, whereas predominantly unilateral ruptures correspond to $\sim 0.5 \leq v_0/v_c \leq 1$. Therefore, by determining the second moments, which specify v_c and v_0, we can differentiate between a rupture similar to Loma Prieta and one similar to Landers.

Data Analysis

We determined the second-degree moments for a catalog of 25 earthquakes with $M_w \geq$7.0 that occurred between 1994 and 1999 (Fig. 2) using the method described by McGuire *et al.* (2001). To isolate an earthquake's finite-source effects, we compared data seismograms with syn-

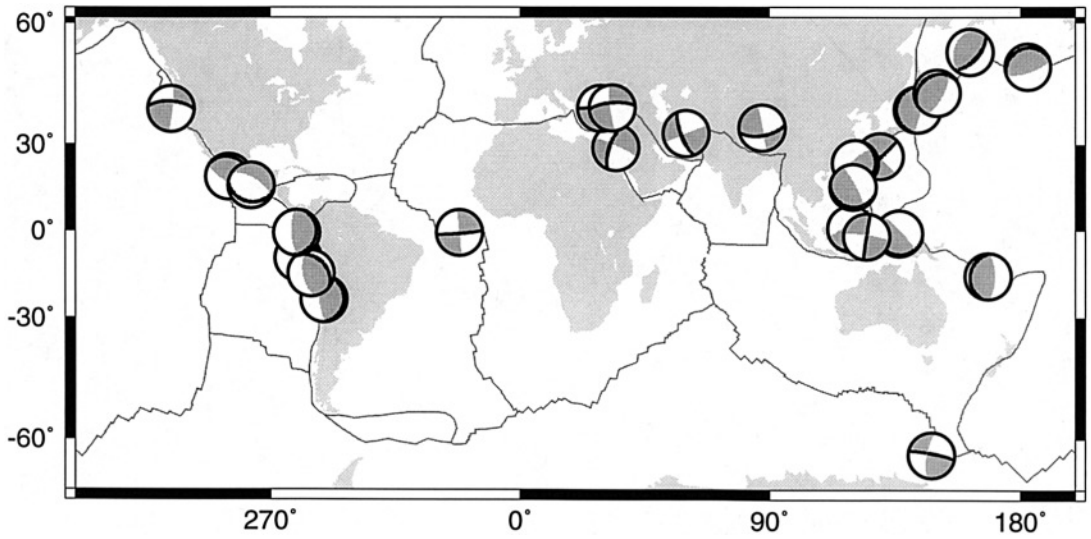

Figure 2. Map showing locations and focal mechanisms of the events in Table 1. Bold nodal planes denote the presumed rupture plane as identified by having the smaller value of $x_c(\hat{n})$, where $\hat{n}$ is the direction normal to the nodal planes (see McGuire *et al.*, 2001). The correct fault plane was identified by this test for 18 of the 19 earthquakes that could be verified by either other studies using local data or by plate boundary geometry. The exception, the 5 December 1997 Kuril earthquake, ruptured primarily along the *N* axis of its focal mechanism, making it more difficult to distinguish between the two nodal planes.

thetics calculated for a point source by normal-mode summation for the preliminary reference earth model (PREM) earth model (Dziewonski and Anderson, 1981), corrected for three-dimensional elastic structure. The small differences between the data and synthetics were quantified for the low-frequency first-orbit Rayleigh and *P* waves as differential phase-delay and amplitude measurements. The differential amplitude measurements primarily result from the second moments (McGuire *et al.*, 2001), which were not incorporated in the point source (zeroth and first moment) synthetics. The differential amplitude and phase-delay measurements were inverted for the second moments as well as for changes to the assumed point-source parameters. Figure 3 shows the differential amplitude measurements for the 1994 Honshu subduction zone thrust earthquake and the 1999 Izmit strike-slip earthquake. The rupture directivity is manifested in these measurements as low-amplitude surface-wave arrivals at the azimuths opposite the primary propagation direction because of the destructive interference these waves experience relative to the amplitude predicted for a point source.

The differential phase-delay and amplitude measurements at low frequencies are linearly related to the second moments. However, a standard linear inversion for the second moments is often very nonunique (see Das and Kostrov, 1997). We stabilized our inversion by incorporating the physical constraint that the four-dimensional source region has nonnegative volume. This constraint, which is an inherent property of all earthquakes, is equivalent to requiring the 4×4 matrix,

$$\begin{bmatrix} \hat{\mathbf{\mu}}^{(2,0)} & \hat{\mathbf{\mu}}^{(1,1)\mathrm{T}} \\ \hat{\mathbf{\mu}}^{(1,1)} & \hat{\mu}^{(0,2)} \end{bmatrix}, \tag{4}$$

to be positive semidefinite. We enforce this constraint on our solution using the semidefinite programming approach of Vandenberghe and Boyd (1996) (see McGuire *et al.* [2001] for more detail). This constraint greatly reduces the nonuniqueness in the second-moment estimation. The largest source of error in our estimates likely results from unmodeled propagation effects. These effects may be correlated for nearby stations. To estimate the size of the uncertainty associated with these and other errors we have used a grouped jackknife method. For the events in this article, we have formed 12 subsets of the data by deleting all the stations within each of 12 30° azimuthal bins. Each of the 12 subsets were inverted using the semidefinite programming algorithm for an estimate of the 10 centroid moment tensor (CMT) and 10 second-moment parameters. These 12 estimates were then combined to estimate the covariance matrix for the model parameters (see McGuire *et al.*, 2001). In Table 1 we present estimates for several quantities that are derived from the second moments using the expressions in equation (3). The uncertainties are derived from the covariance matrix of our second-moment estimates using standard error propagation equations (see Bevington and Robinson [1992], p. 41).

Figure 4 compares our estimates of the 2nd moments for the 17 August M_w 7.4 Izmit, Turkey, earthquake to slip distributions determined with local strong-motion data by Yagi and Kikuchi (2000) and Bouchon *et al.* (2000). Our

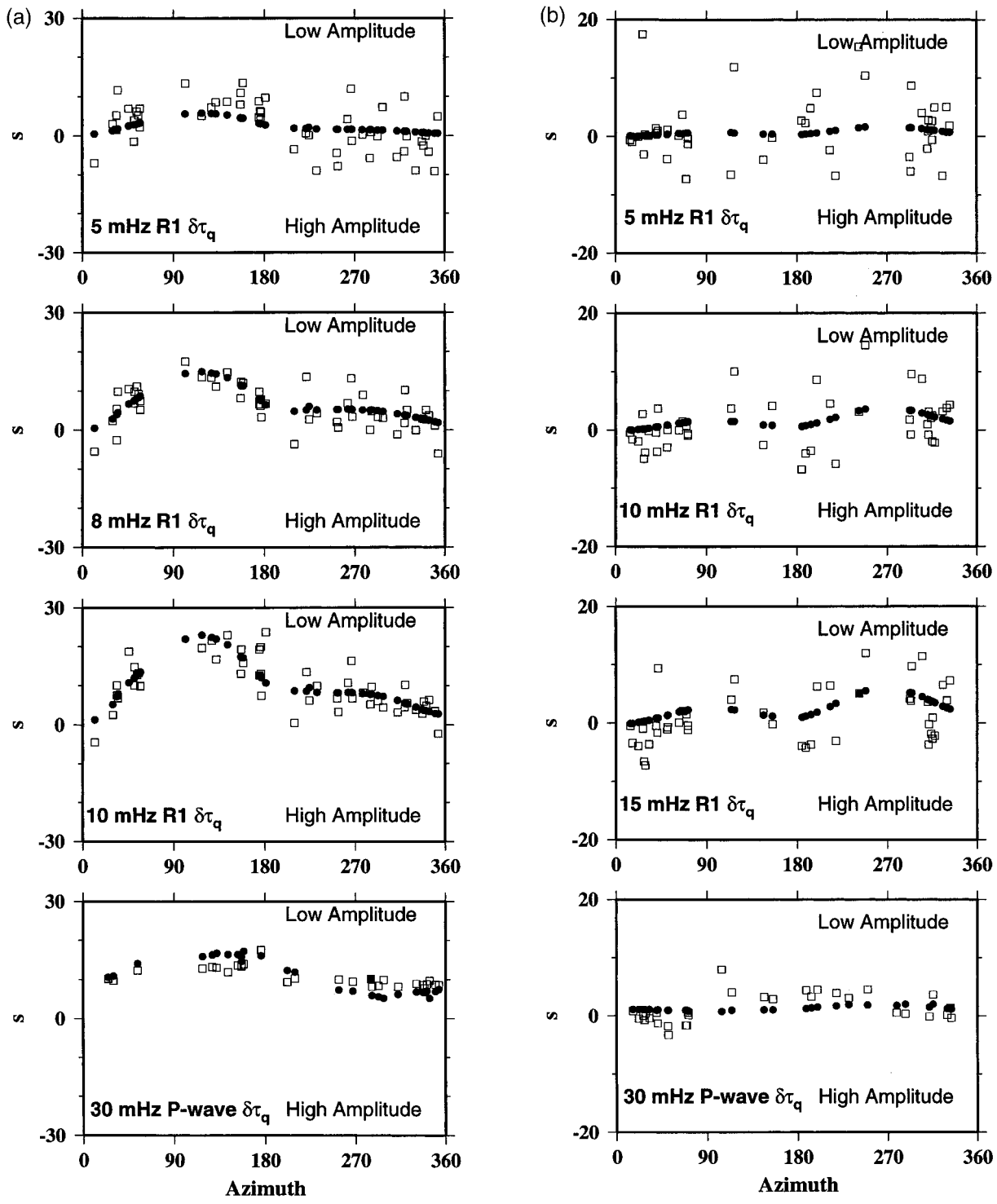

Figure 3. (a) Amplitude measurements ($\delta\tau_p$) for the 1994 Honshu M_w 7.8 earthquake. The open squares are the measurements, and the filled circles are the fit to them by our estimates of the second moments. The low amplitudes at stations to the east indicate that this rupture propagated mainly to the west, namely, in the downdip direction of subduction. The four panels show measurements made at different frequencies on R1 and *P* waves. (b) Amplitude measurements for the 1999 M_w 7.5 Izmit earthquake. The low amplitudes at stations to the east and west indicated a partially bilateral rupture that propagated mainly to the east.

Table 1
Characteristic Rupture Dimensions

Date (mm/dd/yyyy)	Earthquake	M_0 (10^{20} N/m)	L_c (km)	τ_c (sec)	v_c (km/sec)	v_0 (km/sec)	L_0 (km)	Directivity Ratio
09/01/1994	Mendocino	.39	44 ± 4	9 ± 1	4.7 ± 1.4	4.6 ± 1.1	43 ± 3	.99 ± .08
12/28/1994	Honshu	5.7	97 ± 7	19 ± 1	5.0 ± .1	4.6 ± .1	90 ± 3	.93 ± .06
05/18/1994	Romanche	0.2	45 ± 6	13 ± 5	3.6 ± 4.2	3.4 ± 5.1	43 ± 5	.95 ± 1.2
07/30/1995	Chile	20.8	144 ± 14	36 ± 1	4.0 ± .1	2.8 ± .1	102 ± 4	.71 ± .01
10/09/1995	Jalisco	7.4	121 ± 10	29 ± 2	4.1 ± .1	3.7 ± .2	107 ± 7	.88 ± .07
11/22/1995	Aqaba	.69	53 ± 3	12 ± 1	4.5 ± .3	4.3 ± .3	51 ± 2	.97 ± .28
12/03/1995	Kuril	6.2	70 ± 2	25 ± 1	2.8 ± .1	2.4 ± .1	60 ± 2	.86 ± .01
01/01/1996	Minahassa	3.2	127 ± 5	8 ± 2	15.5 ± 3	1.1 ± .6	10 ± 7	.075 ± .12
02/17/1996	Biak	21.7	100 ± 6	18 ± 1	5.6 ± .1	2.2 ± .1	39 ± 2	.39 ± .01
02/21/1996	Peru	2.9	96 ± 4	22 ± 1	4.4 ± .1	1.2 ± .1	27 ± 2	.29 ± .02
06/10/1996	Alaska	7.4	110 ± 7	10 ± 1	10.6 ± .2	7.6 ± .2	79 ± 4	.72 ± .02
11/12/1996	Peru	5.1	87 ± 7	29 ± 1	3.0 ± .1	2.9 ± .1	83 ± 2	.96 ± .01
05/10/1997	Iran	0.93	66 ± 12	17 ± 2	3.9 ± .7	2.9 ± .4	49 ± 6	.74 ± .15
11/08/1997	Tibet	2.2	44 ± 5	10 ± 1	4.4 ± .4	4.3 ± .2	43 ± 4	.99 ± .24
12/05/1997	Kuril	5.3	75 ± 6	28 ± 1	2.7 ± .1	2.6 ± .1	73 ± 4	.98 ± .03
03/25/1998	Antarctica	18.9	178 ± 14	48 ± 1	3.7 ± .1	3.6 ± .1	174 ± 11	.98 ± .02
05/03/1998	Taiwan	2.0	81 ± 4	9 ± 1	8.6 ± .3	2.1 ± .4	20 ± 5	.25 ± .03
08/04/1998	Equador	0.6	62 ± 4	8 ± 1	8.1 ± 2.1	4.5 ± 1.0	34 ± 5	.56 ± .54
11/29/1998	Ceram	2.9	76 ± 5	6 ± 1	12.3 ± 1.6	3.7 ± .6	23 ± 7	.30 ± .09
08/17/1999	Izmit	2.0	52 ± 7	7 ± 1	7.8 ± 1.0	6.3 ± 1.4	42 ± 12	.81 ± .06
09/20/1999	ChiChi	3.6	62 ± 3	12 ± 1	5.3 ± 0.3	2.8 ± 0.1	32 ± 5	.53 ± .13
09/30/1999	Oxaca	2.0	82 ± 5	21 ± 1	3.9 ± .1	2.9 ± .1	60 ± 3	.74 ± .10
11/12/1999	Duece	.56	21 ± 2	4.0 ± 1	5.4 ± 3	4.6 ± 5.5	18 ± 7	.85 ± .50
11/26/1999	Vanuatu	1.9	71 ± 4	25 ± 1	2.8 ± .1	2.8 ± .1	70 ± 3	.99 ± .18
12/11/1999	Luzon	0.8	64 ± 5	7 ± 2	9.8 ± 2.7	6.1 ± 3.6	40 ± 6	.63 ± .67

Errors are ±1 standard deviation.

estimate of L_c, 52 ± 7 km, lies between the values from the two strong-motion inversions (73 and 44 km, Fig. 4). The total rupture length of this earthquake is somewhat uncertain because the western portion of the fault lies underwater (Bouchon et al., 2000). Although the Izmit rupture expanded in both directions along its fault, the average directivity vector, $\hat{\boldsymbol{\mu}}^{(1,1)}$, as estimated by our teleseismic study and as calculated from the strong-motion inversions, pointed to the east because of the greater extent of the rupture in this direction. Our estimated magnitude of the directivity vector, 42 ± 12 km ($L_0 = v_0\tau_0$), is slightly longer than that of either strong-motion inversions (31 and 32 km). The uncertainty in the total rupture length causes the values of the directivity ratio, $v_0/v_c = L_0/L_c$, to be different (.42 versus .73, see Fig. 4) for the two local studies. From these two studies it is clear that the uncertainty in v_0/v_c determined from the local data for this event is comparable to the uncertainty in our teleseismic estimate. The overall agreement in the magnitude and direction of L_c and L_0 for our inversion and the strong-motion studies indicates that we can adequately resolve the character of large earthquake ruptures using only teleseismic data (Fig. 4).

The majority of large earthquakes in our catalog, 20 out of 25, have $v_0 \geq 0.5v_c$, indicating dominantly unilateral ruptures (Fig. 5a, Table 1). Only five events were bilateral ruptures ($v_0 \leq 0.5v_c$) similar to Loma Prieta. We also calculated the directivity ratio for 22 strong-motion inversions for 17 moderate to large earthquakes performed by other authors (Table 2). Only 4 or 5 out of 17 of these earthquakes had directivity ratios less than or equal to 0.5, indicating approximately bilateral ruptures (Fig. 5b). Combining these two datasets shows that the majority of large earthquake ruptures are predominantly unilateral and that the most commonly observed directivity ratios are those between 0.7 and 1.0 (Fig. 6). A ratio of $v_0 \geq 0.5v_c$ appears to be a general feature of large earthquakes.

Potential Mechanisms That Favor Unilateral Rupture

Numerical simulations of dynamic rupture show that a contrast in elastic properties between the two sides of a fault generates an interaction between the normal stress and fault slip that is not present in a homogenous medium (Harris and Day, 1997; Ben-Zion and Andrews, 1998; Ranjith and Rice, 2001). It has been shown that for reguralized friction laws, this interaction produces a preference for unilateral propagation in the direction of slip of the slower medium (Cochard and Rice, 2000; Ben-Zion and Huang, 2001). Rubin and Gillard (2000) proposed that this effect may explain the asymmetric aftershock distributions of small earthquakes found on the central San Andreas fault. Although the details of the elastic structure in the source regions of the events in Table 1 are unknown, they primarily broke plate-boundary faults and hence may have involved material contrasts that

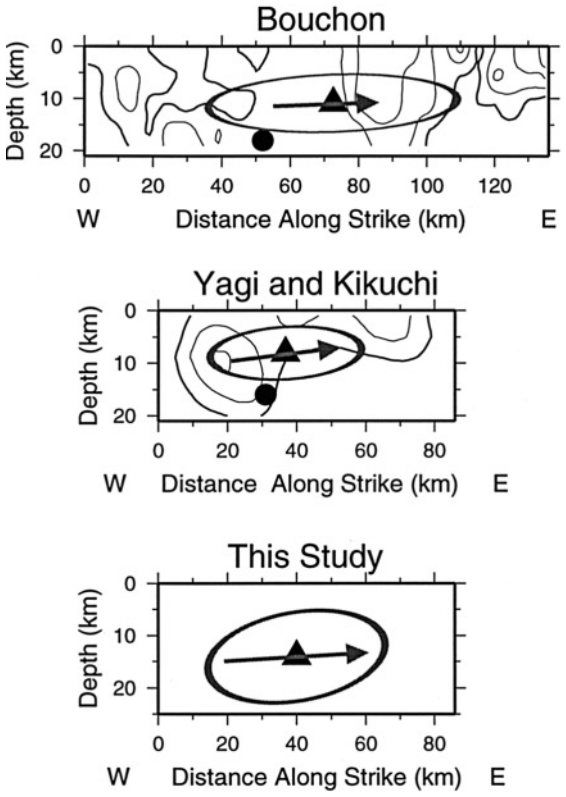

Figure 4. Plots of the second moment values for three studies of the Izmit earthquake (M_w 7.4) (Bouchon *et al.*, 2000; Yagi and Kikuchi, 2000). Triangles denote the centroid locations, and circles denote the epicenters of the studies. Red ellipses denote $\hat{\boldsymbol{\mu}}^{(2,0)}$, and arrows denote $\hat{\boldsymbol{\mu}}^{(1,1)}$ scaled to the length of $v_0\tau_c$ (see McGuire *et al.*, 2001). One-meter contours in the top two panels denote the slip distributions determined by Bouchon *et al.* (2000) and Yagi and Kikuchi (2000) from which the second moments were calculated (Table 2).

favored the abundance of unilateral rupture seen in Figure 5a. One type of plate boundary for which this hypothesis can be considered in more detail is subduction-zone thrust interfaces. The elastic structure surrounding these faults is approximately two-dimensional with little variation along strike. Therefore, if a contrast in elastic properties was responsible for the unilateral ruptures on these faults, their ruptures would propagate dominantly updip or downdip. For instance, if large thrust events rupture the interface between the overlying mantle and the more compliant subducting sediment layer, rupture propagation in the downdip direction would be favored. Thatcher (1989) and Scholz (1990) noted that subduction thrust events often nucleate near the downdip end of the eventual rupture zone, suggesting that updip directivity may be common. Because the material properties of the various subduction interfaces ruptured by the events in our dataset are unknown, we cannot necessarily predict whether updip or downdip rupture should be favored in general. However, because of the two-dimensional nature of subduction interfaces, along-strike rupture would not be favored by this mechanism. There are 12 subduction zone thrust events in Table 1, 9 of which are dominantly unilateral ruptures. For none of these nine events does the directivity vector, $\boldsymbol{\mu}^{(1,1)}$, have an azimuth within $\pm 30°$ of the updip or downdip directions. For seven of these nine events, the azimuth of the directivity vector lies within $\pm 30°$ of the along-strike direction. Thus, material property contrasts are unlikely to be the primary cause of the predominance of unilateral rupture seen in the large, $M \geq 7$, earthquakes in Figure 5a.

The unilateral nature of the subduction ruptures appears to be related to the along-strike length of the seismogenic zone being greater than the downdip width. Moreover, these events appear to nucleae at one end of their eventual rupture area and propagate primarily unilaterally along strike to the other end of this region. Several authors (Mogi, 1969; Kelleher *et al.*, 1974; Scholz, 1990) have noted that subduction zone events tend to nucleate and terminate at structural irregularities that can be recognized as bathymetric features.

The preference for ruptures with $v_0 \geq 0.5v_c$ may also result from preexisting structural controls on rupture size. Large earthquake ruptures are often expected to be stopped at fault segment boundaries (Harris and Day, 1991). The characteristic earthquake model (Schwartz and Coppersmith, 1984; Wesnousky, 1994) predicts that a large earthquake will rupture in both directions along the strike of a fault until it reaches the discontinuities at the end of the fault segment in which the rupture nucleated. We constructed a simple version of this model, a one-dimensional fault where all earthquakes rupture the entire fault with a uniform slip distribution. Thus, the only variable parameter is the location of the epicenter with respect to the fault ends. A uniform distribution of epicenters along the fault leads to a predominance of unilateral rupture for this model. Figure 7 presents the distribution of directivity ratios (L_0/L_c) produced by this one-dimensional fault-segment model. The fault-segment boundaries lead to half of the ruptures propagating at least 3 times as far in one direction as they do in the other, and hence the preference for directivity rations greater than 0.7. Thus, fault-segmentation need only control the termination of rupture to produce the preference for unilateral ruptures seen in our global study.

Uniform slip does not accurately represent most earthquakes. Thatcher (1989) suggested that large subduction earthquakes tend to nucleate near small regions of high slip (asperities). To simulate this potentially more realistic scenario, we added a region of high slip to the one-dimensional fault model described above and nucleated all simulated events at the boundary of the asperity. As long as the asperity length is small ($\leq$20% of fault length, i.e., similar to that observed by Thatcher [1989]) and randomly distributed along the fault, the distribution of directivity parameters remains similar to that shown in Figure 7. However, as the asperity length increases (as a percentage of total fault length), the relative abundance of unilateral ruptures in-

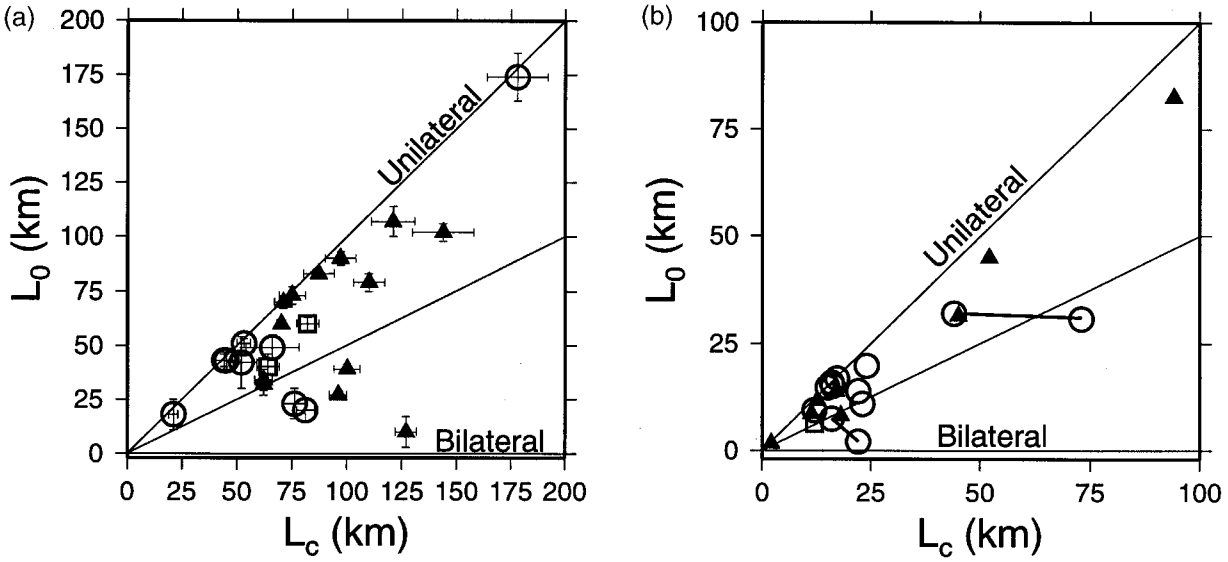

Figure 5. (a) Plot of L_c versus L_0 for the events in Figure 1 and Table 1. Lines denote slopes of 0 (bilateral), 0.5, and 1 (unilateral). Circles denote strike-slip earthquake, triangles denote thrust events, and squares denote dip-slip events. (b) Similar plot for the strong-motion inversions listed in Table 2.

Table 2
Characteristic Rupture Dimensions of Strong-Motion Slip Models

Earthquake	M_0 (10^{20} N/m)	L_c (km)	W_c (km)	τ_c (sec)	v_c (km/sec)	v_0 (km/sec)	v_0/v_c	Reference
Hector Mine	.6	22	5	5.1	4.2	2.7	.64	Ji *et al.* (2001)
Landers	1.05	24	9	9	2.8	2.2	.79	Wald and Heaton (1994)
Northridge	.15	11	9	3	3.5	2.7	.77	Wald *et al.* (1996)
Northridge	.15	12.6	7.4	3.6	3.5	3.2	.91	Dreger (1994)
Sierra Madre	.0025	2.1	1.7	.57	3.5	2.9	.83	Wald (1992)
Izmit	2.9	73	11	11	6.6	2.8	.42	Bouchon *et al.* (2000)
Izmit	2.9	44	10	8	5.5	4.0	.73	Yagi and Kikuchi (2000)
Imperial Valley	.058	16	6	6	2.6	2.4	.92	Archuleta (1984)
Impreial Valley	.058	17	6	6	2.9	2.8	.97	Hartzell and Heaton (1983)
Loma Prieta	.24	16	7	3.7	4.3	2.0	.47	Beroza (1995)
Loma Prieta	.24	22	8	4.2	5.2	0.5	.10	Wald *et al.* (1991)
Morgan Hill	.026	16	5	5.1	3.3	3.1	.95	Beroza and Spudich (1988)
Morgan Hill	.026	15	6	4.6	3.3	3.2	.96	Hartzell and Heaton (1986)
Kobe	.24	23	9	4.7	5.0	2.3	.46	Wald (1996)
Superstition	.035	12	5	9.4	1.2	1.0	.82	Wald *et al.* (1990)
Michoacan	14.	94	75	27.5	3.4	3.0	.88	Mendoza and Hartzell (1988)
NPalmSprings	.017	12	8	2.4	5.0	2.6	.52	Mendoza and Hartzell (1988)
BoraPeak	2.3	22	13	6.8	3.3	3.1	.94	Mendoza and Hartzell (1988)
ChiChi	4.6	45	23	15	3.1	2.1	.68	Ma *et al.* (2001)
Nahanni1	.10	17	8	4.3	3.9	3.2	.82	Hartzell *et al.* (1991)
Nahanni2	.15	18	10	4.5	3.9	1.8	.46	Hartzell *et al.* (1991)
Tabas	.53	52	22	15	3.4	3.0	.88	Hartzell and Mendoza (1991)

The slip distributions were obtained from the U.S. Geological Survey variable-slip, finite-fault source model repository (*http://pasadena.wr.usgs.gov/office/wald/slip_models.html*) and Martin Mai's compilation (personal comm., 2001).

creases owing to the weighted average nature of the second moments. Thus, adding the complexity of slip heterogeneity to this model will only increase the preference for events with $v_0 \geq 0.5v_c$ as long as the ruptures propagate to both ends of the fault.

The second-degree moments provide a clear way to quantify earthquake rupture directivity. Both our study of large earthquakes based on teleseismic data and the studies of moderate to large earthquakes by other authors using strong-motion data indicate that the majority of large earthquakes have a predominantly unilateral rupture with $v_0 \geq 0.5v_c$. Although material property contrasts may explain

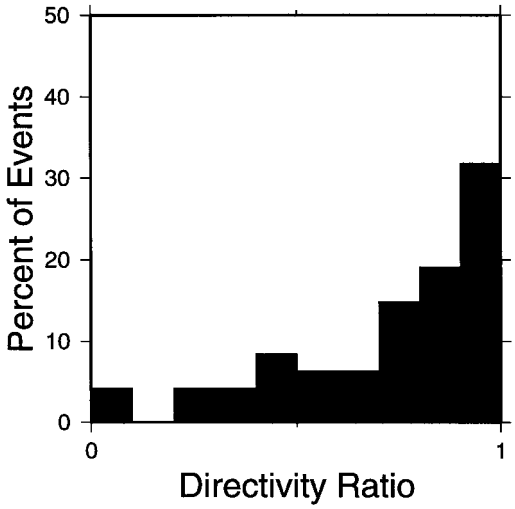

Figure 6. Histogram of the values of the directivity ratio for the events in Tables 1 and 2.

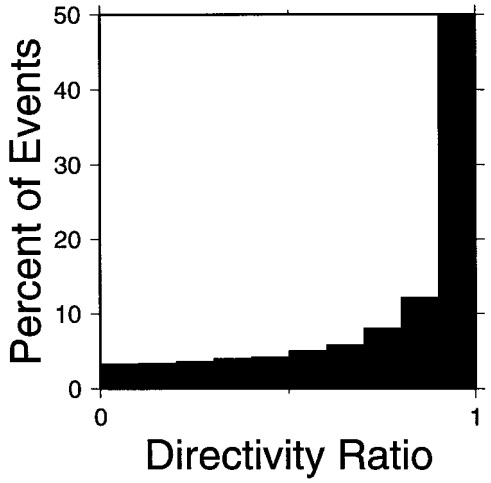

Figure 7. Similar histogram to Figure 6 for simulated ruptures on the one-dimensional fault model described in the text. The epicenters were distributed uniformly and all ruptures propagated to both ends of the fault with a uniform slip distribution.

earthquakes in certain areas, fault-segmentation appears to provide a more likely explanation for the predominance of unilateral rupture we observe in large earthquakes. To explain our observations, it is only necessary for the segmentation to control the termination of large ruptures. If initiation also preferentially occurs at segment boundaries, this would further enhance the predominance of unilateral rupture. Our observations quantify what appears to be a general property of large earthquake dynamics. Because of the large effects of directivity on near-field ground motions, it may be advantageous to build rupture models with $v_0 \geq 0.5v_c$ into seismic hazard estimates.

Acknowledgments

This work was sponsored by the National Science Foundation under grant EAR-9805202. We thank M. Bouchon and Y. Yagi for allowing us to reproduce their slip models of the Izmit earthquake, and D. Wald for maintaining the U.S. Geological Survey finite-source model repository from which the events in Table 2 were taken. We also thank Martin Mai for assistance with the finite-source models and G. Beroza for discussions. This manuscript was prepared with the American Geophysical Union's LATEX macros v5, with the extension package AGU^{++} by P. W. Daly, version 1.5f, from 16 July 1998

References

Archuleta, R. (1984). A faulting model for the 1979 Imperial Valley earthquake, *J. Geophys. Res.* **89,** 4559–4585.

Backus, G. E. (1977a). Interpreting the seismic glut moments of total degree two or less, *Geophys. J. R. Astr. Soc.* **51,** 1–25.

Backus, G. E. (1977b). Seismic sources with observable glut moments of spatial degree two, *Geophys. J. R. Astr. Soc.* **51,** 27–45.

Backus, G., and M. Mulcahy (1976a). Moment tensors and other phenomenological descriptions of seismic sources I. Continuous displacements, *Geophys. J. R. Astr. Soc.* **46,** 341–361.

Backus, G., and M. Mulcahy, (1976b) Moment tensors and other phenomenological descriptions of seismic sources II. Discontinuous displacements, *Geophys. J. R. Astr. Soc.* **47,** 301–329.

Ben-Menahem, A. (1961). Radiation of seismic waves from finite moving sources, *Bull. Seism. Soc. Am.* **51,** 403–435.

Ben-Zion, Y., and D. J. Andrews (1998). Properties and implications of dynamic rupture along a material interface, *Bull. Seism. Soc. Am.* **88,** 1085–1094.

Ben-Zion, Y., and Y. Huang (2001). Dynamic rupture on an interface between a compliant fault zone and a stiffer surrounding solid, *J. Geophys. Res.* **107** (in press).

Beroza, G. C. (1995). Near-source modeling of the Loma Prieta earthquake: evidence for heterogeneous slip and implications for earthquake hazard, *Bull. Seism. Soc. Am.* **81,** 1603–1621.

Beroza, G. C., and P. Spudich (1988). Linearized inversion for fault rupture behavior application to the 1984 Morgan Hill, California earthquake, *Bull. Seism. Soc. Am.* **93,** 6275–6296.

Bevington, P. R., and D. K. Robinson (1992). *Data Reduction and Error Analysis for the Physical Sciences*, McGraw-Hill, New York.

Bouchon, M., N. Toksoz, H. Karabulut, M. Bouin, M. Dietrich, M. Aktar, and M. Edie (2000). Seismic imaging of the 1999 Izmit (Turkey) rupture inferred from the near-fault recordings, *Geophys. Res. Lett.* **27,** 3013–3016.

Bukchin, B. G. (1995). Determination of stress glut moments of total degree 2 from teleseismic surface wave amplitude spectra, *Tectonophysics* **248,** 185–191.

Cochard, A., and J. Rice (2000). Fault rupture between dissimilar materials: Ill-posedness, regularization, and slip-pulse response, *J. Geophys. Res.* **105,** 25,891–25,907.

Dahlen, F. A., and J. Tromp (1988). *Theoretical Global Seismology*, Princeton University, Princeton, New Jersey.

Das, S., and B. V. Kostrov (1997). Determination of the polynomial moments of the seismic moment rate density distributions with positivity constraints, *Geophys. J. Int.* **131,** 115–126.

Dreger, D. S. (1994). Empirical Green's function study of the January 17, 1994 Northridge, California earthquake, *Geophys. Res. Lett.* **21,** 2633–2636.

Dziewonski, A. M., and D. L. Anderson (1981). Preliminary reference Earth model, *Phys. Earth Planet. Inter.* **25,** 297–356.

Harris, R. A., and S. M. Day (1991). Fault steps and the dynamic rupture process: 2-d numerical simulations of a spontaneously propagating shear fracture, *Geophys. Res. Lett.* **18,** 893–896.

Harris, R. A., and S. M. Day (1997). Effects of a low-velocity zone on a dynamic rupture, *Bull. Seism. Soc. Am.* **87,** 1267–1280.

Hartzell, S., and T. Heaton (1983). Inversion of strong ground motion and teleseismic waveform data for the fault rupture history of the 1979 Imperial Valley, California earthquake, *J. Geophys. Res.* **73,** 1553–1583.

Hartzell, S., and T. Heaton (1986). Rupture history of the 1984 Morgan Hill, California, earthquake from the inversion of strong motion records, *Bull. Seism. Soc. Am.* **76,** 649–674.

Hartzell, S., and C. Mendoza (1991). Application of an iterative least-squares waveform inversion of strong motion and teleseismic records to the 1978 Tabas, Iran, earthquake, *Bull. Seism. Soc. Am.* **81,** 305–331.

Hartzell, S., C. Langer, and C. Mendoza (1991). Rupture histories of Eastern North American earthquakes, *Bull. Seism. Soc. Am.* **84,** 1703–1724.

Ji, C., D. J. Wald, and D. V. Helmberger (2001). Source description of the 1999 Hector Mine, California earthquake. II. Complexity of slip history, *Bull. Seism. Soc. Am.* (in press).

Kelleher, J., J. Savino, H. Rowlett, and W. McCann (1974). Why and where great thrust earthquakes occur along island arcs, *J. Geophys. Res.* **81,** 4889–4899.

Ma, K.-F., J. Mori, S.-J. Lee, and S. B. Yu (2001). Spatial and temporal distribution of slip for the 1999 Chi-Chi, Taiwan, earthquake, *Bull. Seism. Soc. Am.* **91,** 1069–1087.

McGuire, J. J., L. Zhao, and T. H. Jordan (2001). Measuring the second-degree moments of earthquake space-time distributions, *Geophys. J. Int.* **145,** 661–678.

Mendoza, C., and S. H. Hartzell (1988). Inversion for slip distribution using teleseismic p waveforms: North Palm Springs, Borah Peak, and Michoacan earthquakes, *Bull. Seism. Soc. Am.* **78,** 1092–1111.

Mogi, K. (1969). Relationship between the occurrence of great earthquakes and tectonic structures, *Bull. Earthquake Res. Inst. Univ. Tokyo* **47,** 429–441.

Ranjith, K., and J. Rice (2001). Slip dynamics at an interface between dissimilar materials, *J. Mech. Phys. Solids* **49,** 341–361.

Riedesel, M. A., and T. H. Jordan (1989). Display and assessment of seismic moment tensors, *Bull. Seism. Soc. Am.* **79,** 85–100.

Rubin, A. M., and D. Gillard (2000). Aftershock asymmetry/rupture directivity among central San Andreas fault microearthquakes, *J. Geophys. Res.* **105,** 19,095–19,109.

Scholz, C. H. (1990). *The Mechanics of Earthquake Faulting*, Cambridge University Press, Cambridge, U.K.

Schwartz, D. P., and K. J. Coppersmith (1984). Fault behavior and characteristic earthquakes: examples from the Wasatch and San Andreas faults, *J. Geophys. Res.* **89,** 5681–5698.

Silver, P. G., and T. H. Jordan (1983). Total-moment spectra of fourteen large earthquakes, *J. Geophys. Res.* **88,** 3273–3293.

Thatcher, W. (1989). Earthquake recurrence and risk assessment in circum-pacific seismic gaps, *Nature* **341,** 432–434.

Vandenberghe, L., and S. Boyd (1996). Semidefinite programming, *SIAM Review* **38,** 49–95.

Wald, D. J. (1992). Strong motion and broadband teleseismic analysis of the 1991 Sierra Madre, California earthquake, *J. Geophys. Res.* **97,** 11,033–11,046.

Wald, D. J. (1996). Slip history of the 1995 Kobe, Japan, earthquake determined from strong motion, teleseismic, and geodetic data, *J. Phys. Earth* **44,** 489–503.

Wald, D. J., and T. H. Heaton (1994). Spatial and temporal distribution of slip for the 1992 landers, california, earthquake, *Bull. Seism. Soc. Am.* **84,** 668–691.

Wald, D. J., T. H. Heaton, and K. W. Hudnut (1996). The slip history of the 1994 Northridge, California, earthquake determined from strong ground motion, teleseismic, GPS, and leveling data, *Bull. Seism. Soc. Am.* **86,** S49–S70.

Wald, D. J., D. V. Helmberger, and S. H. Hartzell (1990). Rupture process of the 1987 Superstition Hills earthquake from the inversion of strong-motion data, *Bull. Seism. Soc. Am.* **80,** 1079–1098.

Wald, D. J., D. Helmberger, and T. H. Heaton (1991). Rupture model of the 1989 Loma Prieta earthquake from the inversion of strong ground motion and broadband teleseismic teleseismic data, *Bull. Seism. Soc. Am.* **81,** 1540–1572.

Wesnousky, S. G. (1994). The Gutenberg–Richter or characteristic earthquake distribution, which is it? *Bull. Seism. Soc. Am.* **84,** 1940–1959.

Yagi, Y., and M. Kikuchi (2000). Source rupture process of the Kocaeli, Turkey, earthquake of August 17, 1999, obtained by joint inversion of near-field data and teleseismic data, *Geophys. Res. Lett.* **27,** 1969–1972.

Department of Geophysics
Stanford University
Stanford, California 94305
(J.M.)

Department of Earth Sciences
University of Southern California
Los Angeles, California 90089
(L.Z., T.H.J.)

Manuscript received 16 November 2001.